AIAA-2001-1236

ON THE ACCURACY OF PROBABILISTIC BUCKLING LOAD PREDICTIONS

Johann Arbocz*
Delft University of Technology, The Netherlands
and
James H. Starnes** and Michael P. Nemeth***
NASA Langley Research Center, Hampton, VA 23681-001

ABSTRACT

The buckling strength of thin-walled stiffened or unstiffened, metallic or composite shells is of major concern in aeronautical and space applications. The difficulty to predict the behavior of axially compressed thin-walled cylindrical shells continues to worry design engineers as we enter the third millennium. Thanks to extensive research programs in the late sixties and early seventies and the contributions of many eminent scientists, it is known that buckling strength calculations are affected by the uncertainties in the definition of the parameters of the problem such as definition of loads, material properties, geometric variables, edge support conditions and the accuracy of the engineering models and analysis tools used in the design phase.

The NASA design criteria monographs [1] from the late sixties account for these design uncertainties by the use of a lump sum safety factor. This so-called "empirical knockdown factor γ" usually results in overly conservative design. Recently new reliability based probabilistic design procedure for buckling critical imperfect shells have been proposed [2,3]. It essentially consists of a stochastic approach which introduces an improved "scientific knockdown factor λ_a", that is not as conservative as the traditional empirical one.

In order to incorporate probabilistic methods into a High Fidelity Analysis Approach one must be able to assess the accuracy of the various steps that must be executed to complete a reliability calculation. In the present paper the effect of the size of the experimental input sample on the predicted value of the scientific knockdown factor λ_a calculated by the First-Order, Second-Moment Method is investigated.

INTRODUCTION

Buckling strength of thin-walled stiffened or unstiffened, metallic or composite shells is of major concern in many aeronautical and space applications. It is well known that the critical buckling load is affected by the uncertainties in the definition of loads, material properties, geometric variables, engineering models and the accuracy of the analysis tools used in the design phase. The NASA design criteria from the late sixties account for these design uncertainties by the use of a lump sum safety factor, the so-called "knockdown" factor γ [1], which usually results in an overly conservative design.

Lately, probabilistic design procedures have been proposed as a viable alternative [2,3]. It is felt that quantifying and understanding the "problem uncertainties" and their influence on the design variables provides an approach which will ultimately lead to a better engineered, better designed and safer structures.

However, the vast majority of practicing engineers agree that true reliability must be demonstrated and not just estimated from analysis. It is the authors' opinion, that before the engineering community will begin in large numbers to accept the current generation of probabilistic tools, two conditions must be satisfied. First, there must be test-constructed data bases which can help in mapping the input parameter uncertainties into probability density functions. In addition, there must be failure data bases, which can be used for test verification of the probabilistic failure load predictions.

* Professor, Faculty of Aerospace Engineering, Associate Fellow AIAA
** Senior Engineer, Structures and Materials Competency, Fellow AIAA
*** Senior Research Engineer, Associate Fellow AIAA

It is generally agreed that, in order to make the development of the Advanced Space Transportation System a success and to achieve the very ambitious performance goals (like every generation of vehicles 10x safer and 10x cheaper than the previous one), one must make full and efficient use of the technical expertise accumulated in the past 50 years or so, and combine it with the tremendous computational power now available. It is obvious that with the strict weight constraints used in space applications these performance goals can only be achieved with an approach often called "high fidelity analysis", where the uncertainties involved in a design are simulated by refined and accurate numerical models. In the end the use of "high fidelity" numerical simulation will also lead to overall cost reduction, since the analysis and design phase will be completed faster and only the reliability of the final configuration needs to be verified by structural testing.

In order to incorporate probabilistic methods into a High-Fidelity Analysis Approach one must be able to assess the accuracy of the various steps that must be executed to complete a reliability calculation.

The central problem in the application of stochastic processes is the estimation of the various statistical parameters in terms of real data. According to Papoulis [4], using ensemble averaging to evaluate the lower order statistical moments is appropriate if a sufficiently large number of realizations of the random vector $\mathbf{X}^{(m)}$ are available.

This paper deals specifically with this problem. To investigate the effect of the size of the input sample on the predicted value of the scientific knockdown factor λ_a, the First-Order, Second-Moment Method [3] is applied successively to sample groups of different sizes.

TEST PROGRAM

Using STONIVOKS [5], a special purpose testing machine developed at the Structures Laboratory of the Faculty of Aerospace Engineering in Delft, a sample of 32 nominally identical seamless stainless steel "beer cans" were tested. Figure 1 shows a typical test specimen before top and bottom are cut off. Figure 2 gives the general dimensions of a typical specimen and shows the variation of the wall thickness along 4 equally spaced generators. Notice the increasing wall thickness towards the open end of the can.

The imperfection surveys of the test-specimen were carried out with the STONIVOKS testing machine of the Delft University of Technology (see Fig. 3). The testing machine mainly consists of a rotating platform on which the test specimen is placed, and a vertical moving pick-up (LVDT transducer). The shell is mounted between two circular end discs. The top and bottom ends of the can are cut off giving a cylinder of length 100 mm. Next this specimen is placed between the end disks in a circular channel which is filled with molten "Cerrobend". When the "Cerrobend" solidifies the edges of the cylinder are fully clamped (Fig. 4). The rotary moment of the platform and the vertical movement of the pick-up are synchronized in such way that one revolution of the specimen corresponds to a vertical displacement of the pick-up by 1 mm. The number of measurements in the circumferential direction is fixed at 100. Since the usefull length of the cylinders is about 80 mm the number of measurements per test is 8000. As the rotary movement of the platform (and subsequently the vertical movement of the displacement pick-up) is continuous, the measuring pattern is a helix over the outside surface of the specimen. Figure 3 shows the specimen installed in its testing position. For a detailed discussion of this apparatus see Ref. [5]. All buckling tests were preceded by a complete imperfection survey controlled and recorded by means of a Hewlett-Packard HP9825S desktop calculator.

Data Reduction

The data reduction process involves 4 steps, namely: interpolation of the experimental data, elimination of the rigid body motions, a best fit correction, and finally a harmonic analysis.

As stated before, the measuring pattern is a helix over the outside surface of the test specimen. In order to make the measurements suitable for a harmonic analysis the imperfection data must be interpolated in axial direction. Considering the error level present in the measured data (due to the measuring system) a linear interpolation is sufficient.

Although production and assembly of the testing machine and the preparation of the test specimen was very accurate, a certain amount of rigid body motion of the test specimen was unavoidable. This rigid body motion is mainly caused by the fact that the center line of the specimen never exactly coincides with the axis

of rotation of the platform. Because the absolute values of the imperfections are small, it is essential to correct the measured imperfection pattern for these rigid body motions. To measure this rigid body motion, a pair of transducers (LVDT's) are used which measure the displacements of the outer rim of the two end disks. The outer rim of each disk is considered to be concentric to a high degree. An analysis of this rigid motion shows that the displacements measured at the outer rim of the end disks may be considered as to be sinusoidal. After calculation of the average displacements of each rim and subtracting this value from the measured displacements on the outer rim of the upper and lower ring a linear interpolation of the measured imperfections in the axial direction is carried out.

Before calculating the coefficients of the double Fourier series representations of the measured contours, it is necessary to determine what is to be considered the perfect shell. This is done by fitting a best-fit cylinder (Fig. 5) to the measured data of the initial imperfection scan. The method of least squares is used to calculate the eccentricities X_1, Y_1, the rigid body rotations $\varepsilon_1, \varepsilon_2$ and the mean radius R. Finally, the initial imperfections are defined by recomputing the measured distances with respect to the newly found "perfect" cylinder. The recalculated radial initial imperfections of the isotropic shell IWI-16 are shown in Fig. 6. The coefficients of the following double Fourier series, referenced to the "best-fit cylinder"

$$\bar{W}^{(m)}(x,y) = t\sum_i A_{io}^{(m)} \cos i\pi\frac{x}{L} \qquad (1)$$
$$+ h\sum_k\sum_\ell \sin k\pi\frac{x}{L}\left(C_{k\ell}^{(m)}\cos\ell\frac{y}{R} + D_{k\ell}^{(m)}\sin\ell\frac{y}{R}\right.$$

are calculated numerically.

By assuming that the Fourier coefficients of the initial imperfections are the basic random variables X_i, we have a sample of 32 random fields representing the 32 nominally identical shells. For further details of the test-data the interested reader should consult Ref. [6].

STOCHASTIC STABILITY ANALYSIS

The collapse problem of axially compressed isotropic cylinders can best be formulated in terms of a response (or limit state) function

$$g(\mathbf{X}) = \Lambda_S(\mathbf{X}) - \lambda \qquad (2)$$

where $\lambda = P/P_C$ is the suitably normalized load parameter, Λ_S is the random collapse load of the shell, and the vector $\mathbf{X}$ represents the Fourier coefficients of the initial imperfections. Clearly the response function $g(\mathbf{X}) = 0$ separates the variable space into a "safe region" where $g(\mathbf{X}) > 0$, and a "failure region" where $g(\mathbf{X}) < 0$. The reliability $R(\lambda)$, or the probability of failure $P_f(\lambda)$ can then be calculated as

$$R(\lambda) = 1 - P_f(\lambda) \qquad (3)$$

where

$$P_f(\lambda) = \text{Prob}\{g(\mathbf{X}) \le 0\} = \int_{g(\mathbf{X})\le 0} \cdots\cdots \int f_{\mathbf{X}}(\mathbf{x})d\mathbf{x} \qquad (4)$$

The limit state function $g(\mathbf{X})$, if so desired, can be determined with great accuracy with currently available nonlinear finite element codes such as STAGS [7]. However, the evaluation of the multi-dimensional probability integral, where the domain of integration depends on the shape of the response (or limit state) function, is by no means trivial.

Using as an approximation the First-Order, Second-Moment Method to evaluate this integral involves linearization of the response function $g(\mathbf{X}) \to Z(\mathbf{X})$ at the mean point and knowledge of the distribution of the random vector $\mathbf{X}$. To combine the use of numerical codes with the mean value First-Order, Second-Moment Method, one needs to know the lower order probability characteristics of Z. In the first approximation the mean value of Z is

$$E(Z) = E(\Lambda_S) - \lambda = E[\Psi(X_1,\ldots,X_n)] - \lambda \qquad (5)$$
$$\sim \Psi[E(X_1),\ldots,E(X_n)] - \lambda$$

whereas the variance of Z is approximated by

$$\text{var}(Z) = \qquad (6)$$
$$\text{var}(\Lambda_S) \sim \sum_{j=1}^{n}\sum_{k=1}^{n}\left(\frac{\partial\psi}{\partial\xi_j}\right)\left(\frac{\partial\psi}{\partial\xi_k}\right)\text{cov}(X_j, X_k)$$

where $\text{cov}(X_i, X_j)$ is the variance-covariance matrix. The calculation of the value of $\psi[E(X_1),\ldots,E(X_n)]$, which is the deterministic collapse load of the imperfect shell with mean imperfection amplitudes, and of the derivatives

$\partial\psi/\partial\xi_j$ (or $\partial\psi/\partial\xi_k$) is done with MIUTAM [8], the code that was chosen for the numerical work. The calculation of the derivatives $\partial\psi/\partial\xi_j$ (or $\partial\psi/\partial\xi_k$) is performed numerically by using the following numerical differentiation formula evaluated at values of $\xi_j = E(X_j)$ (or $\xi_k = E(X_k)$)

$$\frac{\partial\psi}{\partial\xi_j} = \frac{\psi(\xi_1,..,\xi_{j-1},\xi_j+\Delta\xi_j,\xi_{j+1},..,\xi_n) - \psi(\xi_1,\xi_2,..,\xi_n)}{\Delta\xi_j} \quad (7)$$

The mean values and the variance-covariance matrix of the basic random variables X_i are obtained by evaluating the following ensemble averages for a sample of experimentally measured initial imperfections

$$\bar{A}_i^{(e)} = \frac{1}{M}\sum_{m=1}^{M} A_i^{(m)} \quad ; \quad \bar{C}_r^{(e)} = \frac{1}{M}\sum_{m=1}^{M} C_r^{(m)} \quad (8)$$

$$K^{(e)}_{A_iA_j} = \frac{1}{M-1}\sum_{m-1}^{M}[A_i^{(m)} - \bar{A}_i^{(e)}][A_j^{(m)} - \bar{A}_j^{(e)}] \quad (9)$$

$$K^{(e)}_{C_rC_s} = \frac{1}{M-1}\sum_{m-1}^{M}[C_r^{(m)} - \bar{C}_r^{(e)}][C_s^{(m)} - \bar{C}_s^{(e)}] \quad (10)$$

where M is the number of sample shells, and m is the serial number of shells. See Reference [9] for further details.

Having obtained the quantities $E(Z) = E(\Lambda_S) - \lambda$ and Var(Z), one can proceed to estimate the probability of failure $P_f(\lambda)$ as

$$P_f(\lambda) = \text{Prob}(Z<0) = F_Z(0) = \int_{-\infty}^{0} f_Z(t)\,dt \quad (11)$$

where $F_Z(t)$ is the probability distribution function and $f_Z(t)$ is the probability density function of Z.

Assuming that the limit state function Z is normally distributed, then

$$f_Z(t) = \frac{1}{\sigma_Z\sqrt{2\pi}}\exp\left[-\frac{1}{2}\left(\frac{t-a}{\sigma_Z}\right)^2\right] \quad (12)$$

where $a = E(Z)$ and $\sigma_Z = \sqrt{\text{Var}(Z)}$. Further

$$F_Z(0) = \int_{-\infty}^{0} f_Z(t)\,dt = \frac{1}{2} + \text{erf}\left(\frac{-a}{\sigma_Z}\right) = \frac{1}{2} - \text{erf}\left(\frac{a}{\sigma_Z}\right) = \phi(-\beta) \quad (13)$$

where $\beta = a/\sigma_Z$ is the reliability index and $\phi(\beta)$ is the standard normal probability distribution function. The error function $\text{erf}(\beta)$ is defined as

$$\text{erf}(\beta) = \frac{1}{\sqrt{2\pi}}\int_0^{\beta} e^{-t^2/2}\,dt \quad (14)$$

Finally, the reliability $R(\lambda)$ will be estimated as

$$R(\lambda) = 1 - P_f(\lambda) = 1 - \text{Prob}(Z<0) = 1 - F_Z(0) = \frac{1}{2} + \text{erf}(\beta) = \phi(\beta) \quad (15)$$

NUMERICAL RESULTS

For the statistical calculations the data associated with the seamless stainless steel "beer scans", tested in Delft in 1987 during the test program described earlier, are used. The shell properties and test results are given in Table 1.

Relying on the results of earlier investigations of the buckling behavior of the imperfect isotropic shell A-8 [3], it was decided to use the following modified 3-mode imperfection model of Koiter [10] for the collapse load calculations.

$$\frac{\bar{W}}{t} = \bar{\xi}_1 \cos i_{c\ell}\pi\frac{x}{L} + (\bar{\xi}_2 \sin k_1\pi\frac{x}{L} + \bar{\xi}_3 \sin k_2\pi\frac{x}{L})\cos\ell\frac{y}{R} \quad (16)$$

where

$$\bar{\xi}_1 = \Delta_{axi} \; ; \; \bar{\xi}_2 = \Delta_{asy} \; ; \; \bar{\xi}_3 = -\frac{k_1}{k_2}\Delta_{asy} \; ;$$

$$i_{c\ell} = \frac{L}{\pi}\sqrt{\frac{2c}{Rt}} \; ; \; c = \sqrt{3(1-\nu^2)}$$

and k_1 and k_2 are roots of the equation which defines the so-called Koiter circle [11]

$$k^2 \frac{Rt}{2c}\left(\frac{\pi}{L}\right)^2 + \ell^2 \frac{Rt}{2c}\left(\frac{1}{R}\right)^2 - k\sqrt{\frac{Rt}{2c}}\left(\frac{\pi}{L}\right) = 0 \quad (17)$$

The Koiter circle is the locus of a family of modes belonging to the lowest eigenvalue $\lambda_c = 1.0$, where by definition

$$\lambda_c = \frac{N_o}{N_{c\ell}} \; ; \; N_{c\ell} = \frac{Et^2}{cR} \qquad (18)$$

and N_o is the applied axial compressive stress resultant. The circumferential wave number ℓ is chosen such that $k_1 = 1$. This yields the first Koiter triad [8]. The ratios of the amplitudes of the imperfections are chosen such that the direction of the postbuckling path coincides with the path of steepest descent, which yields the most adverse imperfection shape [10].

If the measured initial imperfection is represented by the double Fourier series of Eq (1) then its root-mean-square value is by definition

$$\Delta_{rms}^2 = \frac{1}{2\pi RL}\int_0^{2\pi R}\int_0^{L}[\bar{W}(x,y)]^2\,dxdy \qquad (19)$$

$$= \frac{t^2}{4}\{2\sum_{i=1}^{n_1} A_{io}^2 + \sum_{k=1,\ell=2}^{n_1}\sum^{n_2}(C_{k\ell}^2 + D_{k\ell}^2)\}$$

Thus

$$\left(\frac{\Delta_{rms}}{t}\right)^2 = \frac{1}{2}\sum_{i=1}^{n_1} A_{io}^2 + \frac{1}{4}\sum_{k=1,\ell=2}^{n_1}\sum^{n_2}(C_{k\ell}^2 + D_{k\ell}^2)$$

$$= \Delta_{axi}^2 + \Delta_{asy}^2 \qquad (20)$$

Using the imperfection model of Eq. (16) the corresponding equivalent imperfection amplitudes are listed in Table 2.

In order to investigate the effect of the size of the input sample on the predicted value of the scientific knockdown factor λ_a initially the 32 shells are divided in 8 groups of 4 shells each. Next for every group a separate reliability calculation is carried out using the First-Order, Second-Moment Method (FOSM). When applying this method to the first group of 4 shells each the mean buckling load has to be calculated first. Using the imperfection model of Eq. (16) with the mean values of the corresponding equivalent imperfection amplitudes listed in Table 3, the result of the calculation is $E(\Lambda_s) = 0.550629$.

The derivatives $\partial\psi / \partial\xi_j$ are calculated as follows. For the increment of the random variable in Eq. (7), 1% of the original mean value of the corresponding equivalent Fourier coefficient is used, so that $\Delta\xi_j = 0.01 \cdot E(X_j)$.

The calculated derivatives are listed in Table 4. In this study the increments of the path parameter are chosen in such a way that the limit loads are found accurate to within 0.01%. Next, using the sample variance-covariance matrix displayed in Table 5, one can evaluate the mathematical expectation and the variance of Z. The results of these calculations are $E(Z) = 0.550629 - \lambda$ and $Var(Z) = 0.15108 \cdot 10.^{-3}$. Finally, the reliability is calculated directly from Eq. (15) and is plotted in Fig. 7. Notice that for a reliability of 0.99999, one obtains a scientific "knockdown" factor $\lambda_a = 0.49$. Next the same calculations must be repeated for the other groups. The results of the calculations for the 8 groups of 4 shells each are summarized in Table 6. The results of similar calculations for 4 groups of 8 shells each and for 2 groups of 16 shells each are shown in Tables 7 and 8 respectively. Using all 32 shells as one sample group yields the following results:

$$E(Z) - 0.552342 - \lambda \; ; \; \sigma_Z = 0.0234049$$

and $\lambda_a = 0.44$ for a specified reliability of $R(\lambda) = 0.99999$.

CONCLUSIONS

A comparison of the "scientific knockdown factors λ_a" obtained with the different sample sizes listed in Table 8 indicates, that evaluating the mean values and the variance-covariance matrices via ensemble averaging of experimental data yields accurate results if the sample size is 16 or greater.

Comparing the probabilistic buckling load

$$P_a = \lambda_a P_{c\ell} = 0.44(-7909.734) = -3480.283 \text{ lbs}$$

which has a probability of failure of

$$P_f = 1 - R(\lambda) = 1 - 0.99999 = 0.1 \cdot 10^{-5}$$

with the experimental buckling loads shown in Table 1, it is seen that 3 of the test shells buckled below this value. Thus it is evident that the simple initial imperfection model of Eq. (3) does not model the collapse behavior of the shells tested accurately enough. In view of this

one must conclude that in order to improve the accuracy of the probabilistic predictions to a level required by a "High Fidelity Analysis", one must investigate the role of using more refined mechanical models to calculate the collapse loads and employ more advance methods for evaluating the multidimensional probability integral of Eq. (4).

ACKNOWLEDGEMENT

The research reported in this paper was supported in part by NASA Grant NAG 1-2129. This aid is gratefully acknowledged.

REFERENCES

1. Anonymous, "Buckling of Thin-Walled Circular Cylinders", NASA SP-8007, 1968.
2. Ryan, R.S. and Townsend, J.S., "Application of Probabilistic Analysis/ Design Method in Space Programs. The Approaches, The Status and The Needs", in: Proceedings 34th AIAA/ASME/ ASCE/ AHS/ASC Structures, Structural Dynamics and Materials Conference, April 15-22, 1993, La Jolla, California, AIAA Paper No. 93-1381.
3. Arbocz, J., Starnes, J.H. and Nemeth, M.P., "Towards a Probabilistic Criterion for Preliminary Shell Design", in: Proceedings 39th AIAA/ASME/ASCE/ AHS/ASC Structures, Structural Dynamics and Materials Conference, April 20-23, 1998, Long Beach, California, pp. 2941-2955.
4. Papoulis, A., "Probability, Random Variables and Stochastic Processes", Third Edition, McGraw-Hill International Editions, Electrical & Electronic Engineering Series, Singapore, 1991.
5. Verduyn, W.D. and Elishakoff, I., "A Testing Machine for Statistical Analysis of Small Imperfect Shells", Report LR-357, Delft University of Technology, Faculty of Aerospace Engineering, September 1982.
6. Dancy, R. and Jacobs, D., "The Initial Imperfection Data Bank at the Delft University of Technology - Part II", Report LR-559, Delft University of Technology, Faculty of Aerospace Engineering, June 1988.
7. Brogan, F.A., Rankin, C.C. and Cabiness, H.D., "STAGS User Manual", Lockheed Palo Alto Research Laboratory, Report LMSC P032594, 1994.
8. Arbocz, J. and Babcock, C.D., Jr., "Prediction of Buckling Loads Based on Experimentally Measured Initial Imperfections", Proceedings IUTAM Symposium "Buckling of Structures", B. Budiansky (Ed.), June 17-21, 1974, Harvard University, Cambridge, MA, Springer Verlag, Berlin-Heidelberg-New York, 1976, pp. 291-311.
9. Elishakoff, I. and Arbocz, J., "Reliability of Axially Compressed Cylindrical Shells with General Nonsymmetric Imperfections", Journal of Applied Mechanics, Vol. 52, March 1985, pp. 122-128.
10. Koiter, W.T., Personal Communication, California Institute of Technology, April 1974.
11. Koiter, W.T., "On the Stability of Elastic Equilibrium", Ph.D. thesis (in Dutch), TH-Delft, The Netherlands. H.T. Paris, Amsterdam, 1945. English translation issued as NASA TT F-10, 1967, 833 p.

Table 1 Experimental buckling loads and geometric and material properties of the IW1-shells [6]

	P_{exp}		P_{exp}		P_{exp}		P_{exp}
IW1-16	3.05	IW1-24	4.27	IW1-33	4.03	IW1-42	3.82
-17	3.53	-26	3.99	-34	4.68	-43	3.83
-18	4.50	-27	4.16	-36	4.43	-44	4.23
-19	4.51	-28	4.24	-37	3.55	-45	3.99
-20	3.89	-29	4.49	-38	4.20	-46	3.35
-21	4.01	-30	4.46	-39	4.00	-47	3.51
-22	3.82	-31	4.47	-40	4.08	-48	3.43
-23	4.50	-32	4.01	-41	4.03	-49	3.48

For all shells: $R = 33.0\,mm$; $t = 0.1mm$; $E = 2.08 \cdot 10^5 N/mm^2$; P_{exp} in kN
$L = 100.0\,mm$ $\nu = 0.3$

Table 2 Equivalent imperfection amplitudes

$$\frac{\bar{W}}{h} = \bar{\xi}_1 \cos 32\pi \frac{x}{L} + \bar{\xi}_2 \sin \pi \frac{x}{L} \cos 6 \frac{y}{R} + \bar{\xi}_3 \sin 31\pi \frac{x}{L} \cos 6 \frac{y}{R}$$

where $\bar{\xi}_1 = \Delta_{axi}$; $\bar{\xi}_2 = \Delta_{asy}$; $\bar{\xi}_3 = -3.22581 \cdot 10^{-2} \Delta_{asy}$

Shell	$\bar{\xi}_1$	$\bar{\xi}_2$	$\bar{\xi}_3$	Shell	$\bar{\xi}_1$	$\bar{\xi}_2$	$\bar{\xi}_3$
IW1-16	$9.47549 \cdot 10^{-2}$	0.220433	$-7.11075 \cdot 10^{-3}$	IW1-33	$9.19913 \cdot 10^{-2}$	0.375521	$-1.21136 \cdot 10^{-2}$
-17	$9.56081 \cdot 10^{-2}$	0.263060	$-8.48582 \cdot 10^{-3}$	-34	$7.00014 \cdot 10^{-2}$	0.216141	$-6.97230 \cdot 10^{-3}$
-18	$8.48121 \cdot 10^{-2}$	0.206774	$-6.67014 \cdot 10^{-3}$	-36	$1.02874 \cdot 10^{-1}$	0.277256	$-8.94375 \cdot 10^{-3}$
-19	$8.36917 \cdot 10^{-2}$	0.229631	$-7.40746 \cdot 10^{-3}$	-37	$9.59792 \cdot 10^{-2}$	0.376076	$-1.21315 \cdot 10^{-2}$
IW1-20	$1.00125 \cdot 10^{-1}$	0.246147	$-7.94023 \cdot 10^{-3}$	IW1-38	$7.93719 \cdot 10^{-2}$	0.236075	$-7.61533 \cdot 10^{-3}$
-21	$8.48976 \cdot 10^{-2}$	0.217835	$-7.02694 \cdot 10^{-3}$	-39	$9.00877 \cdot 10^{-2}$	0.251087	$-8.09959 \cdot 10^{-3}$
-22	$9.29430 \cdot 10^{-2}$	0.376792	$-1.21546 \cdot 10^{-2}$	-40	$9.50537 \cdot 10^{-2}$	0.450460	$-1.45310 \cdot 10^{-2}$
-23	$8.53030 \cdot 10^{-2}$	0.259375	$-8.36694 \cdot 10^{-3}$	-41	$1.01069 \cdot 10^{-1}$	0.363866	$-1.17376 \cdot 10^{-2}$
IW1-24	$7.75164 \cdot 10^{-2}$	0.214565	$-6.92146 \cdot 10^{-3}$	IW1-42	$8.30259 \cdot 10^{-2}$	0.147869	$-4.76997 \cdot 10^{-3}$
-26	$9.81626 \cdot 10^{-2}$	0.260537	$-8.40443 \cdot 10^{-3}$	-43	$7.33546 \cdot 10^{-2}$	0.215469	$-6.95062 \cdot 10^{-3}$
-27	$9.92225 \cdot 10^{-2}$	0.306576	$-9.88956 \cdot 10^{-3}$	-44	$8.71149 \cdot 10^{-2}$	0.176853	$-5.70494 \cdot 10^{-3}$
-28	$7.57852 \cdot 10^{-2}$	0.148970	$-4.80549 \cdot 10^{-3}$	-45	$7.77785 \cdot 10^{-2}$	0.248184	$-8.00594 \cdot 10^{-3}$
IW1-29	$1.04704 \cdot 10^{-1}$	0.324469	$-1.04668 \cdot 10^{-2}$	IW1-46	$7.47830 \cdot 10^{-2}$	0.274016	$-8.83924 \cdot 10^{-3}$
-30	$6.66228 \cdot 10^{-2}$	0.250015	$-8.06501 \cdot 10^{-3}$	-47	$8.62856 \cdot 10^{-2}$	0.187197	$-6.03862 \cdot 10^{-3}$
-31	$7.04429 \cdot 10^{-2}$	0.166071	$-5.35713 \cdot 10^{-3}$	-48	$7.67555 \cdot 10^{-2}$	0.187495	$-6.04823 \cdot 10^{-3}$
-32	$8.58714 \cdot 10^{-2}$	0.292634	$-9.43982 \cdot 10^{-3}$	-49	$8.66712 \cdot 10^{-2}$	0.245189	$-7.90933 \cdot 10^{-3}$

Table 3 Values of random imperfections and the sample mean vector

	$X_1(=\bar{\xi}_1)$	$X_2(=\bar{\xi}_2)$	$X_3(=\bar{\xi}_3)$
IW1-16	$9.47549 \cdot 10^{-2}$	0.220433	$-7.11075 \cdot 10^{-3}$
-17	$9.56081 \cdot 10^{-2}$	0.263060	$-8.48582 \cdot 10^{-3}$
-18	$8.48121 \cdot 10^{-2}$	0.206774	$-6.67014 \cdot 10^{-3}$
-19	$8.36917 \cdot 10^{-2}$	0.229631	$-7.40746 \cdot 10^{-3}$
E( )	$8.97167 \cdot 10^{-2}$	0.229975	$-7.41854 \cdot 10^{-3}$

Table 4 Derivatives of $\Lambda_s(\mathbf{X}) = \psi[E(X_1),...,E(X_n)]$

	X_j	$\partial\psi / \partial X_j$
$\bar{\xi}_1 = \bar{W}_{32.0}$	1	-1.6240
$\bar{\xi}_2 = \bar{W}_{1.6}$	2	-0.06349
$\bar{\xi}_3 = \bar{W}_{31.6}$	3	1.9546

Table 5 Sample variance-covariance matrix

	1	2	3
1	$0.40149 \cdot 10^{-4}$		Symmetric
2	$0.87569 \cdot 10^{-4}$	$0.57460 \cdot 10^{-3}$	
3	$-0.28248 \cdot 10^{-5}$	$-0.18538 \cdot 10^{-4}$	$0.59802 \cdot 10^{-6}$

Table 6 Reliability calculation for groups of 4 shells each

Group	E(Z)	σ_Z	λ_a
1	0.550629-λ	0.0122915	0.49
2	0.543369-λ	0.0156275	0.47
3	0.553647-λ	0.0289698	0.42
4	0.560122-λ	0.0369662	0.39
5	0.540552-λ	0.0282565	0.41
6	0.536736-λ	0.0235181	0.43
7	0.571050-λ	0.0080433	0.53
8	0.566009-λ	0.0108056	0.51

Table 7 Reliability calculations for groups of 8 shells each

Group	E(Z)	σ_Z	λ_a
1	0.546944-λ	0.0136657	0.48
2	0.556835-λ	0.0307617	0.42
3	0.538439-λ	0.0241657	0.43
4	0.568504-λ	0.0092468	0.52

Table 8 Reliability calculations for groups of 16 shells each

Group	E(Z)	σ_Z	λ_a
1	0.551832-λ	0.0232321	0.44
2	0.552866-λ	0.0243072	0.44

Table 9 Influence of Sample Size on Reliability Predictions

Groups of 4 shells	Groups of 8 shells	Group of 16 shells	Group of 32 shells
#1 $\lambda_a = 0.49$			
#2 $\lambda_a = 0.47$	#1 $\lambda_a = 0.48$		
#3 $\lambda_a = 0.42$			
#4 $\lambda_a = 0.39$	#2 $\lambda_a = 0.42$	#1 $\lambda_a = 0.44$	
#5 $\lambda_a = 0.41$			
#6 $\lambda_a = 0.43$	#3 $\lambda_a = 0.43$		
#7 $\lambda_a = 0.53$			
#8 $\lambda_a = 0.51$	#4 $\lambda_a = 0.52$	#2 $\lambda_a = 0.44$	#1 $\lambda_a = 0.44$

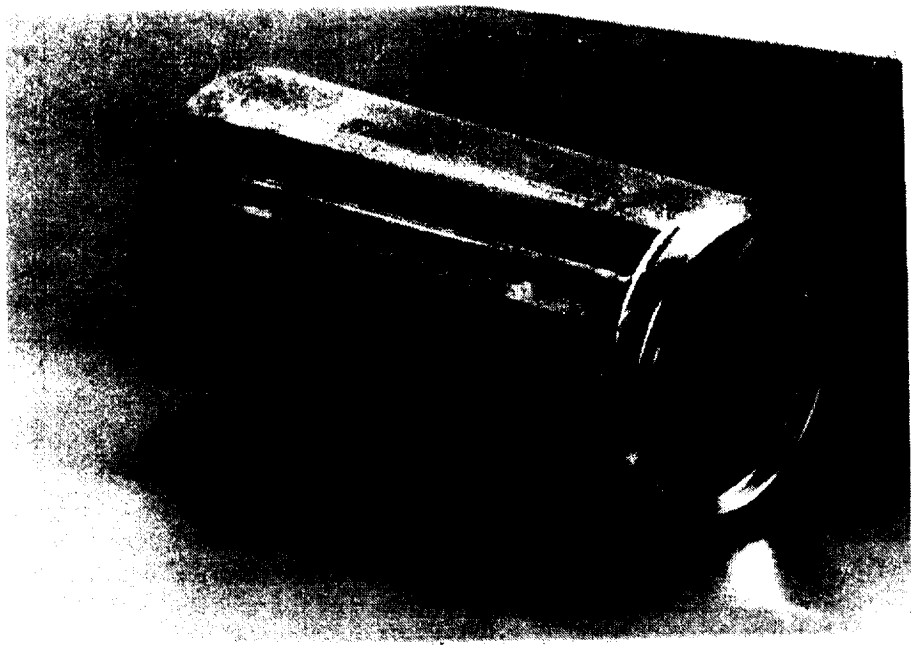

Fig. 1 The original seamless "beer-can" test specimen

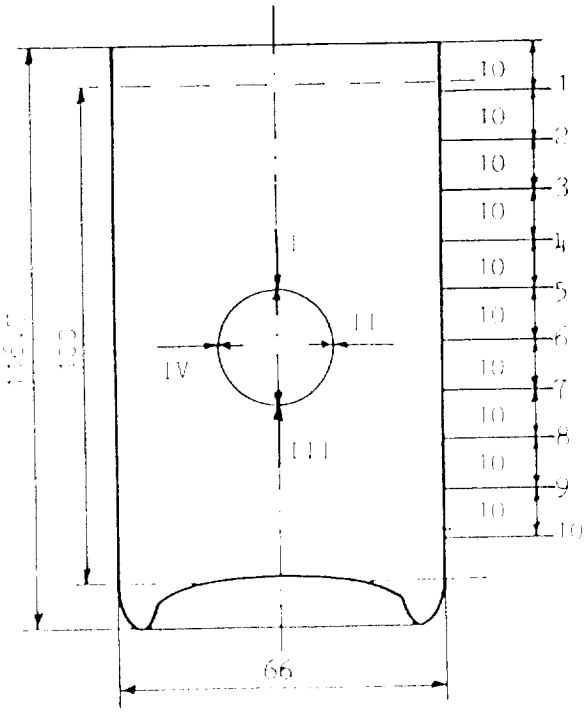

LEVEL	POINT			
	I	II	III	IV
1	.145	.150	.150	.145
2	.130	.130	.130	.130
3	.105	.110	.110	.110
4	.105	.105	.110	.105
5	.105	.100	.105	.105
6	.105	.100	.100	.105
7	.100	.100	.100	.100
8	.100	.100	.100	.100
9	.100	.100	.100	.100
10	.100	.100	.100	.100

[mm]

Fig. 2 General dimensions and wall-thickness distribution of a typical test specimen [5]

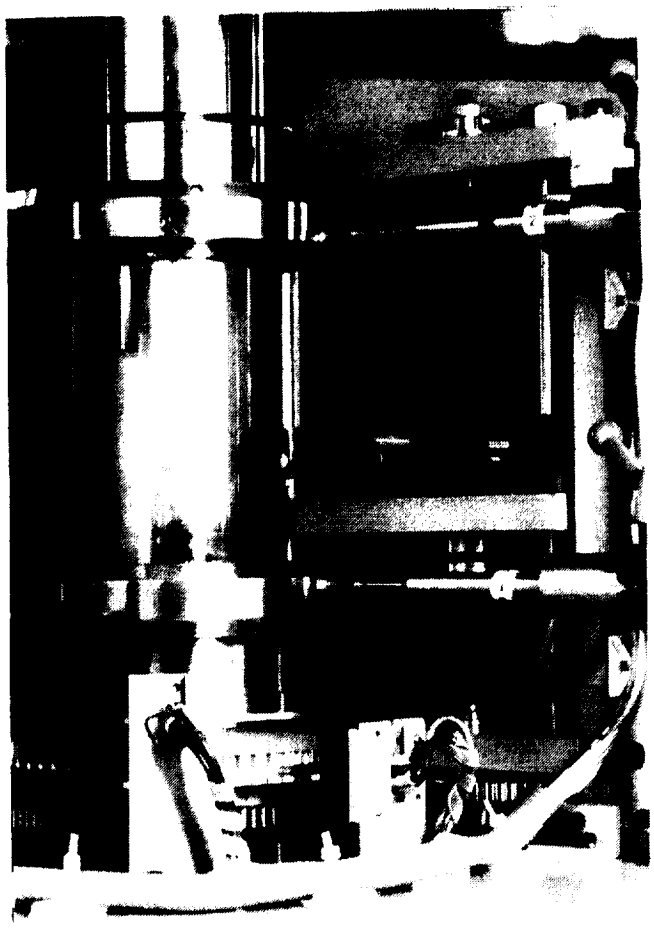

Fig. 3 Displacement pick-ups for contour and rigid body motion measurements [5]

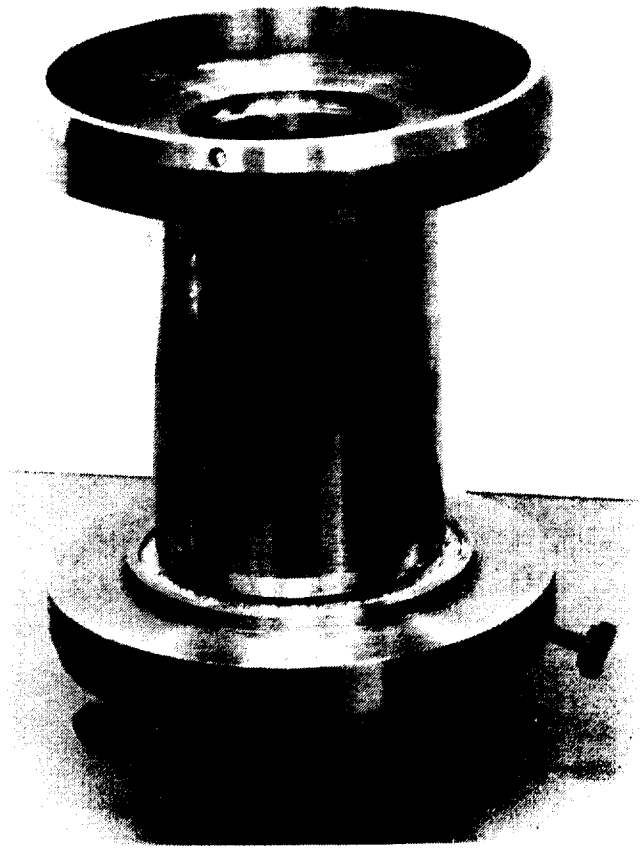

Fig. 4 Test specimen with end disks

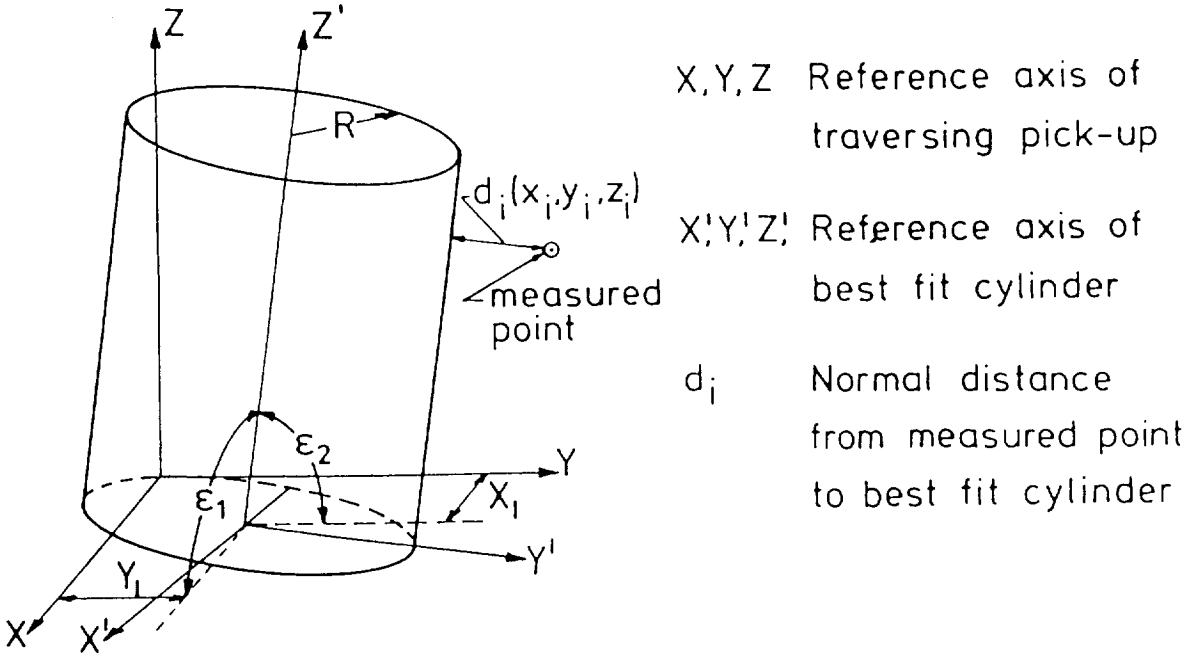

Fig. 5 Best-fit cylinder reference axes

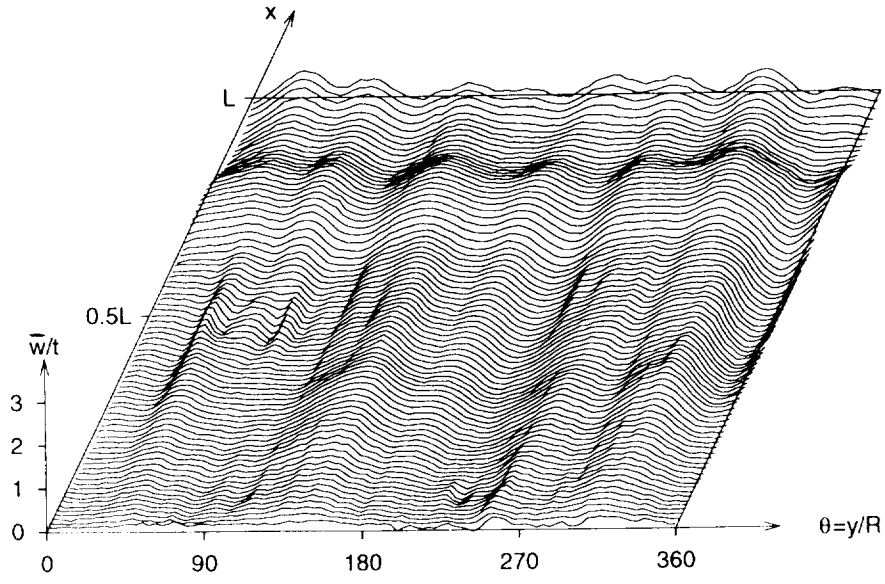

Fig. 6 Measured initial shape of the isotropic shell IW1-16 [6]

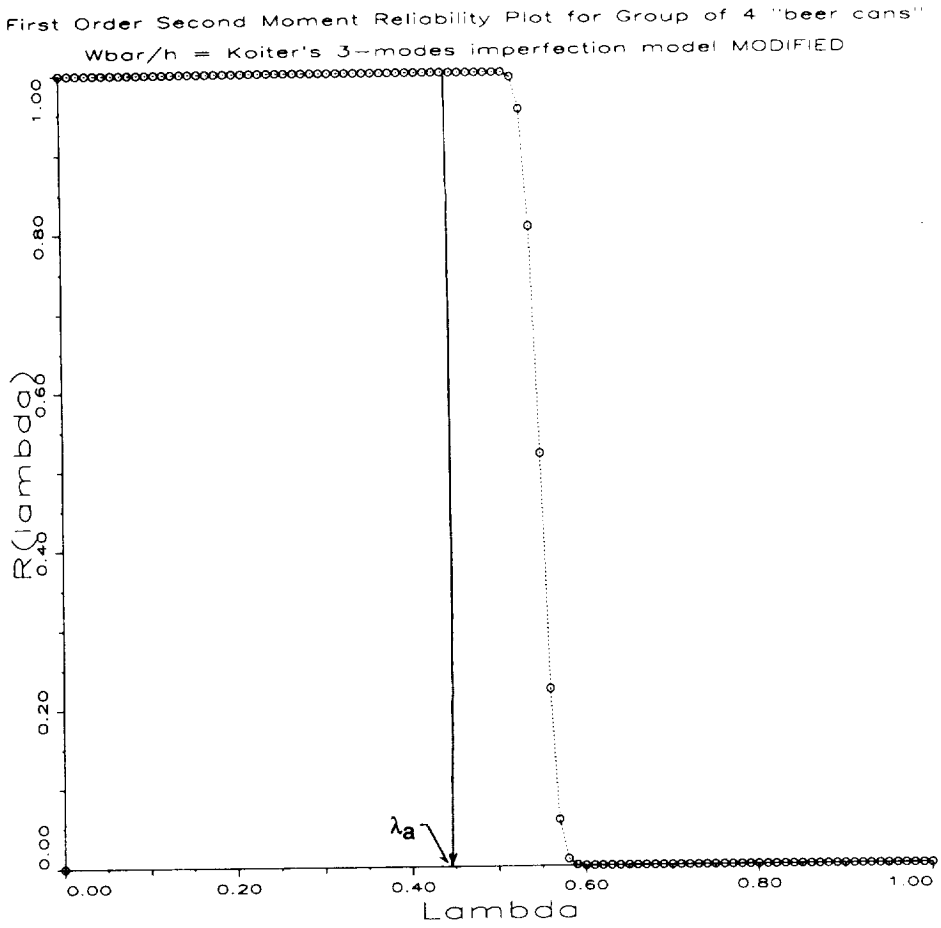

Fig. 7 Reliability of the first group of 4 IW1-shells using Koiter's modified 3-mode imperfection model